Misorientation Changes and Residual Stresses Redistribution after Welding. A Physical Simulation

Tetyana Gurova[a],* [ID], Lincoln Silva Gomes[b], Suzana Bottega Peripolli[b],

Giancarlo Franko Sanchez Chavez[c] [ID], Segen Farid Estefen[d] [ID], Anatoli Leontiev[e] [ID]

[a]Curso de Tecnologia em Construção Naval, Fundação Centro Universitário Estadual da Zona Oeste – UEZO, Rio de Janeiro, RJ, Brasil
[b]Instituto SENAI de Inovação Inspeção e Integridade, Rio de Janeiro, RJ, Brasil
[c]Universidad Nacional de San Agustín - UNSA, Arequipa, Peru
[d]Laboratório de Tecnologia Submarina, Instituto Alberto Luiz Coimbra de Pós-Graduação e Pesquisa de Engenharia - COPPE, Universidade Federal do Rio de Janeiro, Rio de Janeiro, RJ, Brasil
[e]Instituto de Matemática, Universidade Federal do Rio de Janeiro, Rio de Janeiro, RJ, Brasil

Welding is widely used in the manufacture of steel products. Metallurgical processes during welding produce residual stresses in different zones of the welded parts. Welding residual stresses, particularly tensile stresses, can significantly impact the reliability and the integrity of the welded components. Our recent works report the effect of residual stress redistribution in a relatively short, up to two weeks, period after the welding procedure. The hypothesis that the observed stress relaxation phenomenon is associated to the microstructure evolution that occur in the material after the end of the welding procedure was proposed. To prove this hypothesis a physical simulation of the influence of the welding thermal cycles on the base metal with GLEEBLE equipment was performed. Using SEM EBSD, technique the variation of grain boundary misorientation accompanied by the residual stresses redistribution in the first days after welding thermal cycles simulation were observed.

Keywords: *EBSD, grain boundary misorientation, welding stresses, welding, x-ray diffraction.*

1. Introduction

Welding is widely used in the manufacture of steel products. Metallurgical processes during welding, such as shrinkage, quenching, and phase transformations, produce residual stresses in different zones of the welded parts. These residual stresses, particularly tensile stresses, can significantly impact the reliability and the integrity of the welded components. Systematic studies have shown that residual stresses may result in failure mechanisms that are sensitive to localized stresses, such as the following: fatigue, brittle fracture, stress corrosion cracking, and creep cracking. Therefore, it is important to understand the distribution of the residual stresses on the surface of the welded components in and near the welding zone.

Our recent work reports the effect of residual stress redistribution in a relatively short, up to two weeks, period after the welding procedure[1,2,3]. The phenomenon was investigated by the daily monitoring of the welding residual stresses using X-ray diffraction and magnetic methods and the vertical displacements of the welded plate surface with a laser based technology equipment. The observed stress redistribution is characterized by a reduction and a uniformity of the values of the maximum shear stresses 2 weeks after welding. The microstructure analysis rules out the possibility of stress redistribution due to material failure.

The hypothesis that the observed stress relaxation phenomenon is associated to the microstructure evolution that

occur in the material after the end of the welding procedure was proposed[2]. The dislocations originate from crystallisation and deformation processes. Both of these processes occurred during the welding procedure. Afterwards, the accumulation of dislocations can occur. Crystal orientations are changed due to the accumulation of dislocations and may exhibit fluctuations of several degrees, even within the same grain[4]. Thus, the accumulation of dislocations is expected to change the distributions of grain orientations and grain boundary misorientation angle. The formation of dislocations in solids requires energy and introduces residual stresses[5]. During plastic deformation, individual grains do not deform independently of each other and an excess of dislocations is observed at grain boundaries[6]. The accumulation of dislocations in large grains is bigger than in smaller grains, and stress concentration is higher in grains adjacent to larger grains. This means, for example, that in steels containing fine grain structure, greater stress has to be applied to cause slippage across the contour than in coarse grain steels[7].

A direct relationship exists between the level of residual stresses presented in the material and grain boundary misorientation angle[8]. For low angle grain boundaries, the samples with higher stress levels have a higher percentage of misorientation. For high angle grain boundaries, the observed behavior is the opposite. This is corresponds to the fact that the energy of the low angle grain boundaries is the total energy of the dislocations within the contour area and depends on the dislocation spacing. For high angle grain

boundaries, grain boundary energy is almost independent of misorientation[9]. The microstructure evolution is considered as a residual stress forming process in polycrystalline ceramics[10]. During formation of the microstructure, boundaries with higher mobilities and energies are likely to be eliminated, thereby changing the distribution of lattice orientations and grain misorientations. For multicrystalline silicon thin film, it was observed that stresses relax by generating recombination active extended defects such as dislocations and grain boundaries[11].

To prove this hypothesis a physical simulation of the influence of the thermo-mechanical processes on the base metal during the welding thermal cycles was performed with GLEEBLE equipment. The microstructure similar to intercritical coarse grained heat affected zone (IC CGHAZ) near to the fusion zone in a real multi pass welding joint was obtained. Using Electron Backscatter Difraction (EBSD) technique the variation of grain boundary misorientation in the first days after simulation were observed on IC CGHAZ area. These changes were accompanied by the residual stresses redistribution on the heat affected zone (HAZ) region. Residual stress measurements were performed with X-ray diffraction method.

2. Experimental Procedure and Techniques

The samples of dimension 10 x 10 x 71 mm were manufactured from ASTM DH36 steel. The material yield stress is 360 MPa. The chemical composition of the steel is given in Table 1.

A physical simulation of the influence of the welding thermal cycles on microstructure of base metal was performed with GLEEBLE 38000 machine. The specimen was maintained rigidly clamped in the machine jaws, as in Figure 1. The temperature was measured using a K-type thermocouples spot-welded in the middle of the specimen.

The thermal cycles simulation of double pass welding consists of following scheme. The middle region of the test specimen was heated to 1350°C with cooling rate of 450°C/s, and is held at this temperature for 0.35s, then cooled down to 800°C in 20s with cooling rate of 27,5°C/s and then to 200°C in 160s with cooling rate of 3,75°C/s for the first welding pass simulation. The second pass simulation involves heating from 200°C to peak temperature of 800°C with cooling rate of 266°C/s with holding at this temperature for 0.35s and next cooling to 200°C in 160s with cooling rate 3,75°C/s following by air free cooling, as showing in Figure 2.

This thermal scheme was chosen to obtain the microstructure similar to IC CGHAZ near to the fusion zone in the real multi pass welding joint, by simulating, two thermal passes. The
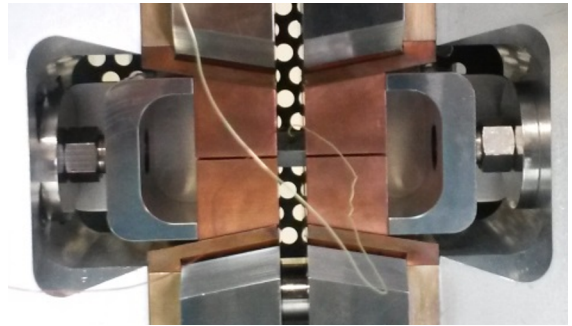
Figure 1. The specimen (in the center of the picture) clamped on the GLEEBLE machine.
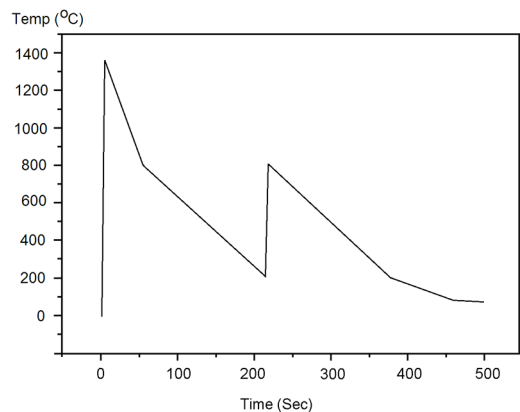
Figure 2. Two pass welding thermal cycles simulation scheme

second thermal pass peak temperature was taken between A_{C1} = 714°C and A_{C3} = 847°C, with the values A_{C1} and A_{C3} calculated by empirical formula[12].
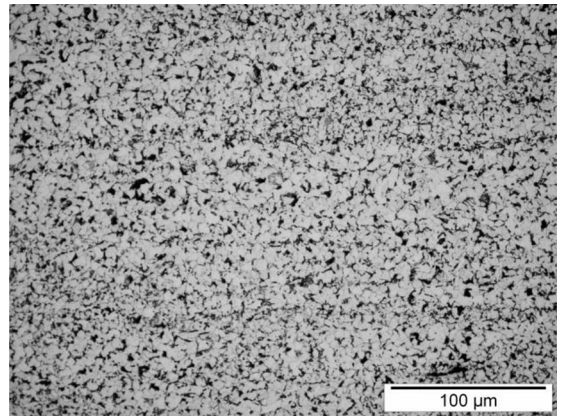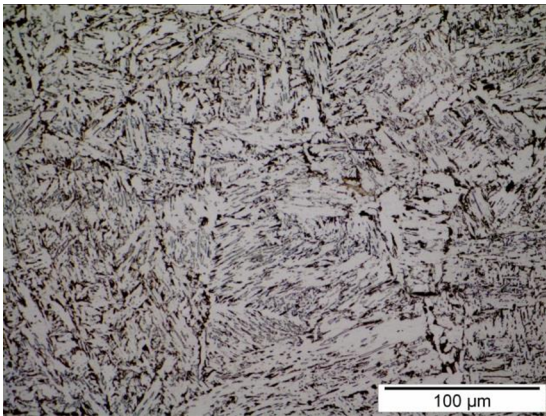
Microstructure of the central part of the specimen, as shown in Figure 3, is compatible with microstructure of IC CGHAZ region in real multi-pass welded samples, shown in Figure 4-a, followed by fine grain heat affected zone (FGHAZ) located at 5 mm from the center of the specimen, Figure 4-b. The FGHAZ was exposed at the temperature to 900°C. The microstructure of the unheated base metal is presented in Figure 5.


Figure 3. Simulated specimen (figure bottom part). The IC CGHAZ area is situated in the central parte of the specimen and has the length of approximately 8 mm. Reference rule (figure top part) in mm

Table 1. Chemical composition of the ASTM DH36 steel in wt.%

C%	Mn%	Si%	Al%	S%	P%	Nb%	V%	Cr%	Cu%	N%
0.141	1.49	0.179	0.393	0.0102	0.0224	0.0322	0.0429	0.0220	0.0106	0.0071

Figure 4. Microstructure of the specimen surface after GLEEBLE simulation, obtained with amplification in 500X with optical microscope: a) central part of the specimen, IC CGHAZ area; b) FGHAZ located at 5 mm from the center of the specimen
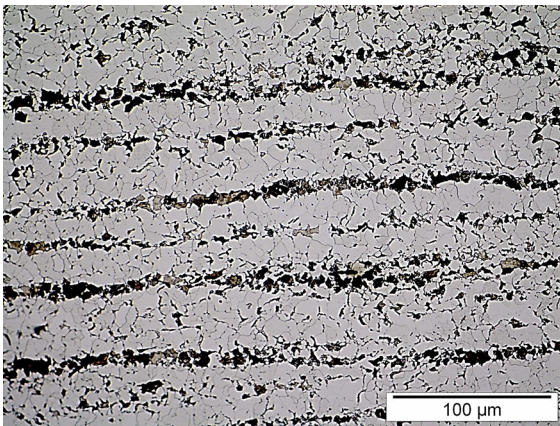

Figure 5. Microstructure of the unheated base metal, amplification in 500X with optical microscope

For data acquisition FEI Quanta 450 scanning electronic microscope (SEM) with tungsten filament and BRUKER E-FLASH EBSD automatic detector were used. BRUKER ESPRIT 2.0 package was applied for data processing. The standard polishing procedure was performed to prepare the specimens for microstructure analysis[13].

The fist specimen was continuously maintained in the vacuum chamber of SEM in the same position for four days and the second one for seven days. The EBSD scanning of IC CGHAZ area was performed each day at the same time, without any equipment settings changes. In both cases, first scanning was made around two hours after the end of GLEEBLE simulation. For the first specimen, EBSD data were collected on 588.5x507.6 µm scan area, with 500x magnification, 0.74 µm step size, a 70° specimen tilt, using working distance of 15.5 mm, high voltage 25.0 kV and a scanning time of 1:16:59 hr. For the second specimen, EBSD data were collected on 73.62 x 63.55 µm scan area with 2000x magnification and 0.72 µm step size, a 70° specimen tilt, using working distance of 16.3 mm, high voltage 20.0 kV and 1:47 hr measurement time for each scanning.

The residual stress values were measured using a RAYSTRESS instrument, which is a portable X-ray equipment that uses the method of double exposure[1,2]. The principle of the stress measurements via the RAYSTRESS using double exposure is shown in Figure 6. Two cassette windows capture the diffraction lines in 2θ-angular intervals from 148° to 164°. The inclination of the specimen surface of 12° corresponds to measurements for steel specimens using Cr-K$_\alpha$ radiation and the {211} reflection with θ_{211}=78°. The experimental accuracy of the stress measurements is 10 MPa.
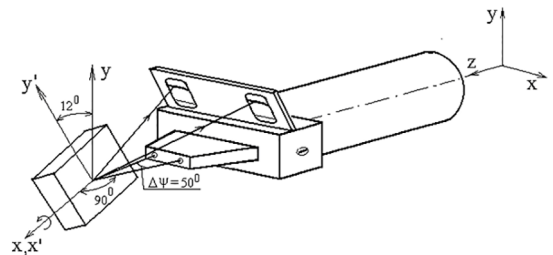
Figure 6. Scheme of the stress measurements using the RAYSTRESS equipment

Specimen was maintained at the same measurement position throughout the all monitoring period of the three weeks. Stresses measurements were made in the center of the specimen on IC CGHAZ area, and on the area located 5 mm from the center of the specimen, whose microsturcture was identified as FGHAZ. The measurements on bouth the areas were performed simultaneously using two RAYSTRESS equipment. Measurements were started arround two hours after the end of the GLEEBLE simulation and were performed every 12 hours.

3. Results and Discussions

3.1 Residual stress redistribution

Figure 7 present the results of residual stresses measurements performed on IC CGHAZ and FGHAZ areas of the specimen during the 21 monitoring days. Sign "-" denotes

the compressive stress. The measurements were performed in the longitudinal direction. Although the stress state on the whole is defined as a tensor value, these measurements are sufficient for the aim of this paper to detect the change of the residual stress state on the analyzed areas.
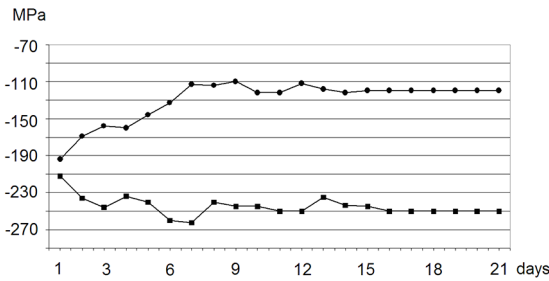
Figure 7. Change in residual stress with time. Plot with ● corresponds to the residual stresses measured on IC CGHAZ area; plot with ■ corresponds to the residual stresses measured on FGHAZ area

We observe the decreasing of the compressive residual stress on IC CGHAZ area accompanying by the increasing of the compressive residual stress on FGHAZ area. This process is not monotonic and has some oscillations. The initial difference of the values of the stresses on two analyzed areas is 20 MPa, and the final difference is 130 MPa. Stabilization in the process of stresses redistribution begins from the second week. Two weeks stabilization period is normally observed in the real welding samples[1,2,3].

3.2 Misorientation changes

It is assumed that the residual strain manifests as local variation in lattice orientation[14], and with increasing strain, low angle grain boundaries generate and their densities increase[15]. Hence local misorientaions provide an indication of the residual strain distribution in the crystalline materials and for its characterizing kernel based methods as Kernel Average Misorientation (KAM) is suitable[14].

Analysis of the EBSD results based on KAM parameter is presented in the Figures 8, 9 and 10. The KAM results were obtained by calculating the difference in orientation from pixels three steps away in each direction (square) up to an orientation cut off of 5 degrees. A visible change of KAM was observed on the last monitoring day. This change consists on increasing of the fractions of angles grain boundaries that are less than 1.25 degrees and decreasing of the fractions of angles grain boundaries that are greater than 1.25 degrees. Thus, the redistribution of residual strain on the IC CGHAZ area of the specimen is detected.

Some authors seek for correlation between the level of residual stresses and the misorientation angles, relating that the specimen with highest absolute stress values has the highest fraction of misorientations present for low boundary angles (less that 15 degrees) and for high angle boundaries an opposite tendency is observed. The conclusion about
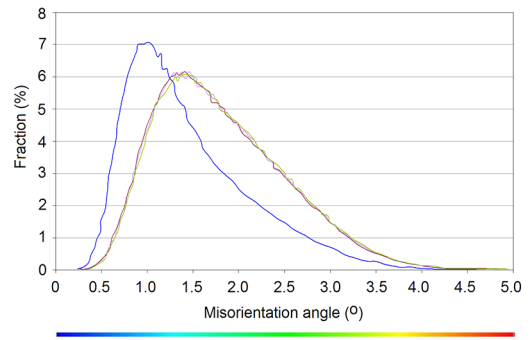
Figure 8. KAM changes on IC CGHAZ area during the four days monitoring and angle reference color scale. Graphics colors: 1-st day - violet; 2-nd day - purple; 3-th day - yellowgreen; 4-th day - blue
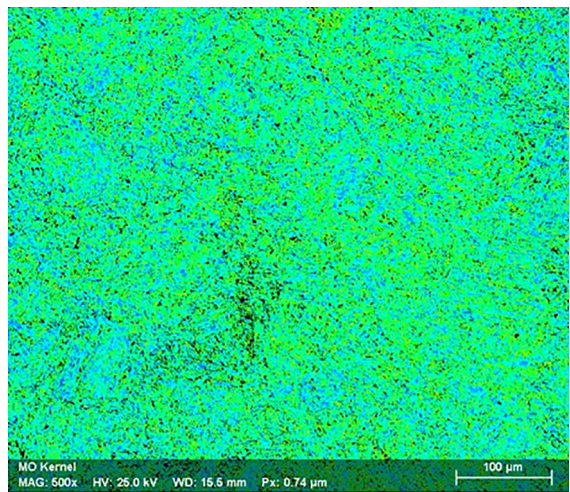

Figure 9. First day monitoring KAM map
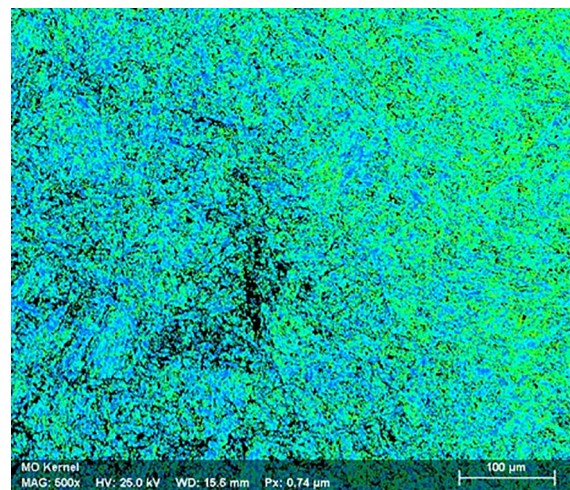
Figure 10. Fourth day monitoring KAM map

residual stresses level is based on the measurement of the stress in one direction only and the correlation results were observed for ASTM A106 Gr B steel[8]. It is worth noting that higher fractions of misorientation for high boundary angles is observed also in the annealed specimens[16].

To observe the correlation between the variation of the residual stresses after welding and the changes in misorientation angles, for the second specimen, the seven day EBSD monitoring was performed. We note that on the first days of monitoring the compressive residual stresses measured in the longitudinal direction on IC CGHAZ area has value 195 MPa and seven day after this value becomes 112 MPa, i.e. absolute value of the residual stress decreases from first to seven day. Then, from first to seventh monitoring days we can have diminution of low boundary angles misorientation fractions and increasing of high boundary angles misorientation fractions[8]. We observe this result for over all phases misorientation angle distribution in the interval from 5 to 45 degrees, Figure 11, and also for misorention of angle grain boundary distribution of ferrite phase, except the angels of degrees more that 55, Figure 12. Indeed, the influence of the ferrite phase, that is a greatest phase, is a principal on the over all phase misorientaion angle distribution result.
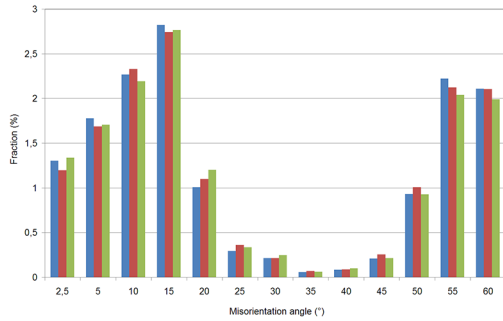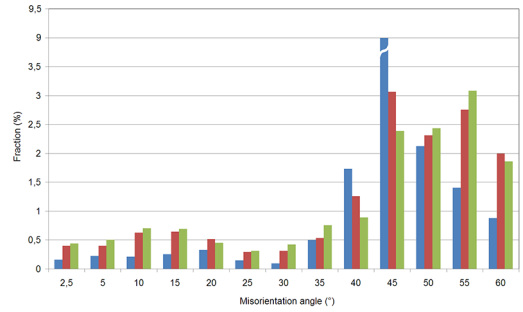

Figure 11. Misorientation angle distribution. 1-st (column at the left), 4-th (column at the middle) and 7-th (column at the right) days of monitoring
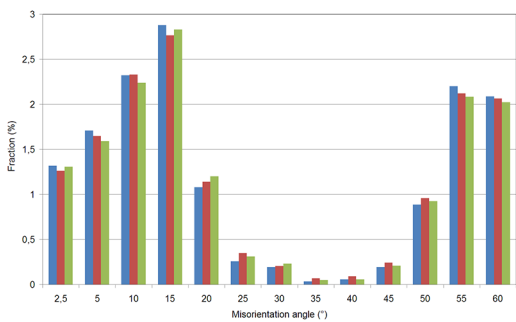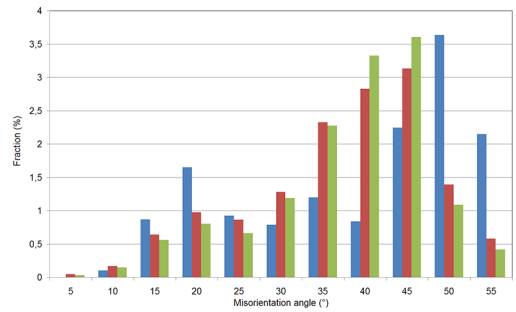

Figure 12. Misorientation angle distribution for ferrite, ccc. 1-st (column at the left), 4-th (column at the middle) and 7-th (column at the right) days of monitoring

The retained austenite, Figure 13, and upper bainite, Figure 14, present well defined opposite tendencies of boundary angles misorientation fraction changes for the angles of 15, 20, 25, 40, 45, 55 degrees.

Comparing the 1-st and 7-th days, we can observe that the misorientation angle distribution for retained austenite and cementite, Figure 15, presents the same character of changes, except 35 degrees misorientation angle.

Figure 13. Misorientation angle distribution for retained austenite. 1-st (column at the left), 4-th (column at the middle) and 7-th (column at the right) days of monitoring

Figure 14. Misorientation angle distribution for upper bainite. 1-st (column at the left), 4-th (column at the middle) and 7-th (column at the right) days of monitoring
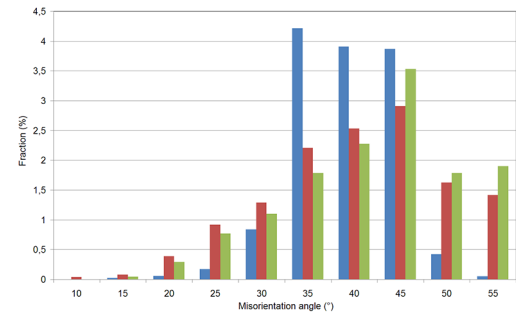
Figure 15. Misorientation angle distribution for cementite. 1-st (column at the left), 4-th (column at the middle) and 7-th (column at the right) days of monitoring

The summary of the misorientation grain boundary angle fraction changes from first to seventh days is given in Table 2. Here "+" denotes increasing and "-" denotes decreasing of the boundary angle misorientation fraction from 1-st to 7-th days. Signal "○" marks the absence of the fraction for comparison. Over all phases misorientation changes is compatible with the expected trend for the interval from 5 to 45 degrees. The expected trend means that for low angle grain boundaries, the samples with higher stress levels have a higher percentage of misorientation. For high angle grain boundaries, the observed behavior is the opposite[8]. Decreasing of misorientation for low angle grain boundary and its increasing for high angle grain boundaries correspond to decreasing of the absolute value of residual stresses measured at IC CGHAZ.

Table 2. Boundary angles misorientation fractions changes. 1-st day vs. 7-th day

Phase	Misorientation angle (o)												
	2.5	5	10	15	20	25	30	35	40	45	50	55	60
Ferrite, ccc	-	-	-	-	+	+	+	+	+	+	+	-	-
Ret. austenite, fcc	+	+	+	+	+	+	+	+	-	-	+	+	+
Upper bainite	○	+	+	-	-	-	+	+	+	+	-	-	○
Cementite	○	○	○	+	+	+	+	-	-	-	+	+	○
All phases	+	-	-	-	+	+	+	+	+	+	-	-	-
Expected	-	-	-	-	+	+	+	+	+	+	+	+	+

The changes tendency for over all phases boundary angles misorientation fractions is following the ferrite one. Only for 2.5 and 50 degrees this tendency is slightly broken by increasing of the retained austenite misorientation fraction and decreasing of the upper bainite misorientation fraction, respectively. Over all phases changes is compatible with the expected trend for the interval from 5 to 45 degrees.

4. Conclusions

The results reported above demonstrate that the effect of residual stresses redistribution observed after welding is accompanied by a change in misorientation at least on IC CGHAZ area, simulated in this study. During the first two weeks after simulation, the compressive residual stress is decreasing on IC CGHAZ area and increasing on FGHAZ area, then the stabilization of this process occurs. At the same time we observe the changes on local misorientations and misorientation angle distribution for each phase and over all phases togehter. Over all phases misorientation changes is compatible with the expected trend for the interval from 5 to 45 degrees. We emphasize that the misorientation changes that occur after welding procedure has not been studied or reported previously in the literature.

5. Acknowledgements

6. References

1. Estefen SF, Gurova T, Werneck D, Leontiev A. Welding stress relaxation effect in butt-jointed steel plates. Marine Structures. 2012;29(1):211-225.

2. Gurova T, Estefen SF, Leontiev A, Oliveira FAL. Welding residual stresses: A daily history. Science and Technology of Welding and Joining. 2015;20:616-621.

3. Gurova T, Estefen SF, Leontiev A, Barbosa PT, Oliveira FAL. Time-dependent redistribution behavior of residual stress after repair welding. *Welding* in the *World*. 2017;61(3):507-515.

4. Shawish SEL, Cizelj L, Simonovski I. Misorientation effects in an anisotropic plasticity finite element model of a polycrystalline under tensile loading. In: 21st International Conference Nuclear Energy for New Europe. Ljubljana, Slovenia; 2012 sep 5-7. Ljubljana, Slovenia: Nuclear Society of Slovenia; 2012. p. 602.1-602.8.

5. François D, Pineau A, Zaoui A. Mechanical Behaviour of Materials, Micro- and Macroscopic Constitutive Behaviour. New York: Springer; 2012. v. 1.

6. Merrimam CC. Orientation dependence of dislocation structure evolution of aluminum alloys in 2-D and 3-D [dissertation]. Washington, DC: Washington State University School of Mechanical and Materials Engineering; 2007.

7. Reed-Hill RE. Physical metallurgy principles. New York: Litton Educational Publishing; 1973.

8. Costa ADSB, Abreu HFG, Miranda H, Costa RCS, Teixeira L, Philipov S. Comparing between residual stresses and grain boundary engineering for tubulations used in hydrodessulfuration systems. In: 4th Congress on P&D Oil and Gas. Campinas, São Paulo, Brasil; 2007 out 21-24. Campinas (SP): 4o PDPETRO; 2007. p. 1-10.

9. Porter DA, Easterling KE, Sherif MY. Phase transformations in metals and alloys. Boca Raton: CRC Press Book; 2009.

10. Vedula VR, Glass SJ, Saylor DM, Rohrer GS, Carter WC, Langer SA, et al. Residual-stress predictions in polycrystalline alumina. Journal of the American Ceramic Society. 2001;84:2947-2954.

11. Sarau G, Becker M, Bochmann A, Gawlik A, Andrä G, Christiansen S. Evolution of residual stress and its relation to microstructure in multicrystalline silicon thin film solar cells on glass prepared by combined laser crystallization and solid phase epitaxy. In: 24th European Photovoltaic Solar Energy Conference, Hamburg, Germany; 2009 sep 21-25. Hamburg, Germany: PVSEC; 2009. p. 2494-2499.

12. Andrews KW. Empirical formulae for the calculation of some transformation temperatures. *Journal of* the *Iron* and *Steel* Institute.1965;203:721-727.

13. Nowell MM, Witt RA, True BW. EBSD sample preparation: techniques, tips, and tricks. Microscopy and Microanalysis. 2005;S2:44-48.

14. Wright SI, Nowell MM, Field DP. A review of strain analysis using electron backscatter diffraction. Microscopy and Microanalysis. 2011;17(3):316-29.

15. Ha JH, Jee KK, Oh KH. Orientation rotation behavior during in situ tensile deformation of polycrystalline 1050 aluminum alloy. *International Journal* of *Mechanical* Sciences. 2003;45(10):1613-1623.

16. Ranjbarnodeh E, Weis S, Hanke S, Fisher A. EBSD characterization of the effect of welding parameters on HAZ of AISI 409. Journal of Mining and Metallurgy Section B-Metallurgy. 2012;48(1):115-121.